

## Article

# Microstructure and Properties of Al-Based Ceramic Coating Deposited on Magnesium Alloy Surface by Cold Spraying

Shiwei Ci <sup>1,†</sup>, Ting Wang <sup>2,†</sup>, Jiaqi Hu <sup>1</sup>, Zonghui Cheng <sup>1</sup>, Suijie Xie <sup>1</sup>, Xiaoye Cai <sup>1</sup>, Dingping Dong <sup>1</sup>, Chao Fan <sup>1</sup>, Qingwei Liu <sup>1</sup>, Chenfeng Yuan <sup>1</sup>, Wenbo Du <sup>3</sup>, Guofeng Han <sup>3</sup>, Sheng Zhu <sup>3</sup>, Dexin Chen <sup>4,\*</sup>  and Qiwei Wang <sup>4,\*</sup>

<sup>1</sup> Anhui Laboratory of Aeronautical Equipment Measurement, Control and Reverse Engineering, State-Owned Wuhu Machinery Factory, Wuhu 241007, China; swcidr@163.com (S.C.)

<sup>2</sup> Vaccine Industry Research Institute, Jinan University, 601 Huangpu Avenue West, Guangzhou 510632, China; 13902216388@139.com

<sup>3</sup> National Key Laboratory for Remanufacturing, Academy of Army Armored Forces, Beijing 100072, China

<sup>4</sup> Institute of Advanced Wear & Corrosion Resistant and Functional Materials, Jinan University, 601 Huangpu Avenue West, Guangzhou 510632, China

\* Correspondence: dxchen@jnu.edu.cn (D.C.); wangqiwei@jnu.edu.cn (Q.W.)

† These authors contributed equally to this work.

**Abstract:** In this study, pure Al and Al-Al<sub>2</sub>O<sub>3</sub> composite coatings with a low porosity and high density were prepared on magnesium alloys by cold spraying. The surface morphology, component, hardness, interfacial bonding, wear and corrosion properties were investigated. Additionally, the relationship between the interface structure and the protective coatings' quality was preliminarily established. Pure Al powder was used to create a coating with a homogeneous and dense microstructure. The hard-phase Al<sub>2</sub>O<sub>3</sub> in the composite coatings was non-oxidized and would reduce the porosity of the coatings to improve their density and interfacial bonding by up to 55.82 MPa. The bonding mode of the pure Al coatings is primarily mechanical, whereas the bonding mode of the Al-Al<sub>2</sub>O<sub>3</sub> mixed coatings is mechanical and metallurgical. The tough Al<sub>2</sub>O<sub>3</sub> particles combined to form a layer of work-hardening reinforcement that resisted wear and effectively prevented it from spreading. The three Al-based coatings had excellent corrosion properties, as evidenced by their corrosion current being several orders of magnitude lower than that of the magnesium alloy substrates. The thick coating was significantly more corrosion-resistant than the thin coating and provided greater protection to the substrate. This study offers theoretical and technological assistance for the surface protection of magnesium alloy equipment in demanding conditions.

**Keywords:** Al-based ceramic coating; cold spraying; magnesium alloys; surface protection



**Citation:** Ci, S.; Wang, T.; Hu, J.; Cheng, Z.; Xie, S.; Cai, X.; Dong, D.; Fan, C.; Liu, Q.; Yuan, C.; et al. Microstructure and Properties of Al-Based Ceramic Coating Deposited on Magnesium Alloy Surface by Cold Spraying. *Coatings* **2023**, *13*, 779. <https://doi.org/10.3390/coatings13040779>

Academic Editor: Jose Luis Viesca

Received: 17 March 2023

Revised: 8 April 2023

Accepted: 12 April 2023

Published: 17 April 2023



**Copyright:** © 2023 by the authors. Licensee MDPI, Basel, Switzerland. This article is an open access article distributed under the terms and conditions of the Creative Commons Attribution (CC BY) license (<https://creativecommons.org/licenses/by/4.0/>).

## 1. Introduction

Magnesium alloy is a typical lightweight metal material, with the advantages of a high specific strength and stiffness, good thermal conductivity and electromagnetic shielding, being recyclable, etc. Known as the “21st-century green engineering materials”, it is widely used in aerospace, automotive manufacturing and other fields [1–3]. The standard electrode potential of magnesium and magnesium alloys is −2.37 V, the corrosion resistance is poor and the mechanical properties are low, which greatly limits their further application [4–6].

Currently, the common failure modes of Mg components involve corrosion, cracking and wear [7]. Researchers have developed a variety of methods for coating magnesium alloy objects, including electroplating, chemical/physical vapor deposition, anodizing, micro-arc oxidation, thermal spraying and cold spraying [8–12]. For instance, to increase the corrosion resistance significantly, a strong, superhydrophobic, dual-layer coating was formed on a Mg alloy by electrodeposition and spraying [13]. By detonation spraying, Zhai et al. synthesized a Fe-based amorphous coating on AZ31B [14]. The distinctive, disordered structure, uniform chemical composition and production of a homogeneous passive coating

on the surface to thwart the invasion of chloride ions and prevent further corrosion were primarily responsible for the outstanding corrosion resistance. Using supersonic plasma spray, Al-coating with a nano-Ti polymer was applied to AZ91-alloy [15]. Due to the development of wrapped routes of a nano-Ti polymer coating and a passivation layer of dense Al coating, the composite coating demonstrated outstanding corrosion resistance.

Compared to other technologies, cold spraying is known for its excellent deposition efficiency and ability to efficiently recover powder [16,17]. On a AZ91 alloy, Zhu et al. used cold spraying to produce a CoCrFeNi high-entropy alloy (HEA) coating with superior wear and corrosion resistance [18]. A modified cold spray technique was used to deposit the high-purity Al and AlMgSi alloy coatings on Mg alloys, increasing their corrosion resistance and fatigue lifespan [19]. Additionally, the addition of Al<sub>2</sub>O<sub>3</sub> to cold-sprayed coatings effectively increased the corrosion and wear resistance [20–22]. This is due to the fact that the addition of alumina particles would improve the bonding and deposition quality to produce outstanding composite coatings [23–25].

In this study, a high-performance pure aluminum coating and an Al-Al<sub>2</sub>O<sub>3</sub> hybrid coating with small porosity and a high density were prepared on the surface of a magnesium alloy using the high-speed and low-temperature characteristics of cold spraying technology for the needs of surface protection and the repair of magnesium alloy material equipment. SEM and EDS were used to characterize the organization of the coating and the interface, to analyze the oxide content, inclusions and porosity and to study the process of forming the coating with different compositions for analysis. The microhardness and bond strength of the coating were measured using a microhardness tester and a universal tensile tester, for example. The tribological properties of the coating, such as its friction coefficient and wear rate, were measured using multi-functional friction and wear testers, and the organization structure change pattern of the wear marks was analyzed by combining SEM and EDS to determine the wear loss mechanism. To investigate the corrosion behavior of the matrix and various coatings under various salt spray times, the polarization curves and impedance spectra of the coatings in a NaCl solution were measured using an electrochemical workstation, and the corrosion characteristics of a magnesium alloy matrix and an aluminum–silicon alloy cold-sprayed layer were compared using a salt spray test.

## 2. Experimental

### 2.1. Materials

ZM5 magnesium alloy was chosen as the matrix material. The powder materials included A0050, A0082 Al-Al<sub>2</sub>O<sub>3</sub> mixed powder and A5001 pure Al powder (Centerline Ltd., Windsor, ON, Canada). Table 1 displays the powder composition and particle size dispersion.

**Table 1.** Parameters and details of powders.

| Powder | Content                             | Purity   | Diameter |
|--------|-------------------------------------|--|----------|
| A5001  | Al                                  | Al 99.5%   | 5~45 µm  |
| A0050  | Al + Al <sub>2</sub> O <sub>3</sub> | Al 99.5%, Al <sub>2</sub> O <sub>3</sub> 92%           | 5~45 µm  |
| A0082  | Al + Al <sub>2</sub> O <sub>3</sub> | Al 99.5% Min, Al <sub>2</sub> O <sub>3</sub> 99.0% Min | 5~75 µm  |

### 2.2. Preparation of Coating

The ZM5 magnesium alloy was wire-cut into samples with dimensions of 30 × 30 × 10 mm<sup>3</sup> and 25.4 × 10 mm<sup>2</sup>. The samples were then submerged in acetone for 30 min to remove any oil, dust or other contaminants from the plate. Finally, the plate was sandblasted to remove the oxide layer, oil and dust. The coating was prepared using the SST-P series portable cold spray system from Centerline Ltd., Windsor, Canada, with the process parameters shown in Table 2.

**Table 2.** Spraying process parameters.

| Parameters           | A5001      | A0050                 | A0082      |
|----------------------|------------|-----------------------|------------|
| Gas temperature      | 400–500 °C | 300–550 °C            | 300–500 °C |
| Gas pressure         |            | 100–250 psi           |            |
| Spraying Distance    |            | 10–25 mm              |            |
| Gas type             |            | Air or N <sub>2</sub> |            |
| Powder feed rate     |            | 12–20 g/min           |            |
| Gun movement speed   |            | 10–500 mm/s           |            |
| Surface pretreatment |            | Sandblasting          |            |

### 2.3. Characterize

The original surface, polished surface and cross-section of the coating were observed and analyzed using scanning electron microscopy (SEM, PHILIPS, Amsterdam, The Netherlands) to study the microstructure of the surface and the cross-section of the coating. The chemical composition of the coating was measured using the attached energy dispersive spectrometer (EDS, X-MaxN20, Oxford Instruments, Abingdon, UK). ImageJ software (v1.48u, 2014, ImageJ, NIH, Rockville, MD, USA) was used to determine the porousness percentage of the coating as well as the porosity of the coating's surface and cross-section. After polishing of the magnesium alloy substrate, coating surface and cross section, the nano-hardness of the magnesium alloy substrate and coating was tested on a KEYSIGHT Nano Indenter (Colorado Springs, CO, USA) nano-hardness tester. The experimental load was 25 g, and the holding time was 15 s. According to the national standard ASTM C 633-79, the coating's bonding strength was tested on an electronic testing device (CMT5000) by Shenzhen New Sansi Material Testing Co., Ltd. (Shenzhen, China), and the VersaSTAT 3 electrochemical workstation (Ametek, Berwyn, PA, USA) was used to measure the potentiodynamic polarization curves and impedance spectra of the samples in the solution (3.5% NaCl aqueous solution). The working electrode was the sample, the reference electrode was the saturated calomel electrode and the auxiliary electrode was the graphite electrode. The sample was stabilized in the solution for 30 min during the test. The scanning rate was 0.5 mV/s after the open circuit had stabilized.

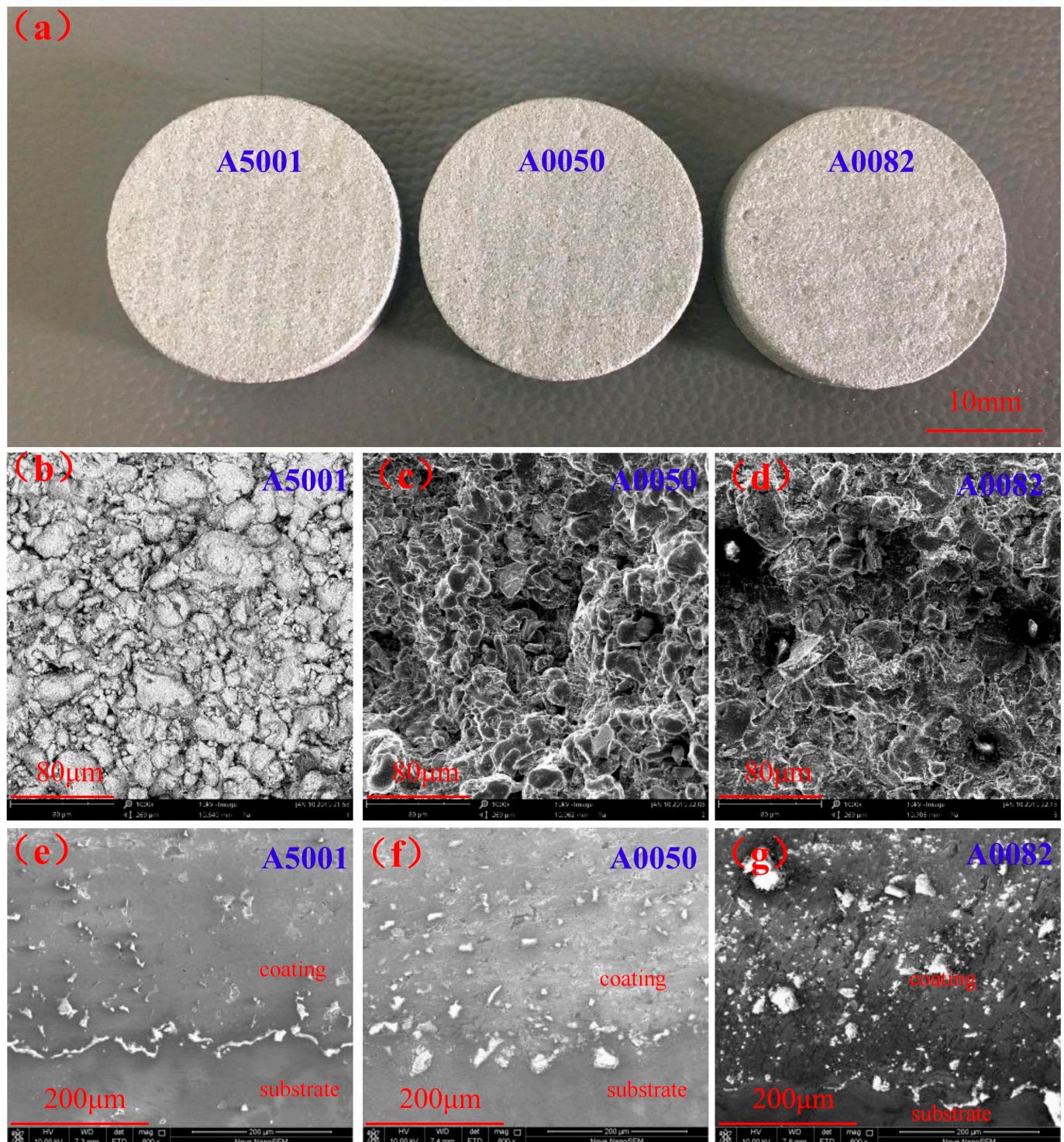
## 3. Result and Discussion

### 3.1. Surface Morphology

A macromorphology image of the coating surface produced by three distinct powders is shown in Figure 1a. From the image, it can be seen that the coating surface is solid, completely silver-gray and free of cracks, pores and other flaws. The surfaces of the thin coatings prepared from the three different compositions of powders were all relatively smooth and flat, with no obvious pits or bumps. The coating made from pure Al powder had an SEM surface morphology (Figure 1b) with a particle diameter of 5–45 µm. The coating's surface is shown to be uneven, to have a large number of pores and to have surface particles that are fractured to varied degrees. The particles come in a variety of sizes. Numerous spherical particles embedded in the coating are present on the surface without evident deformation or fracture. Due to its entirely spherical shape, this particle supports the surrounding component but could also generate a coating porosity. The coating mixture was primarily implanted mechanically. The coating surface produced by the Al-Al<sub>2</sub>O<sub>3</sub> mixed powder had a fairly homogeneous particle size (particle diameter of 5–45 µm) (Figure 1c). The coating had fewer pores than the pure Al powder. Only a small number of particles could preserved the entirety of the particles' form since they were strongly bound together. The majority of the particles were shattered to varied degrees as a result of the hard-phase, high-speed Al<sub>2</sub>O<sub>3</sub> bombarding other particles, which had a significant compaction effect on the coating. The particle underwent plastic deformation, losing its spherical shape and becoming flat. The particles' high kinetic energy was simultaneously transformed into heat energy, causing localized melting and the formation



of metallurgical bonds between the particles. Mechanical interlocked and metallurgical bonding are primarily estimated as the coating's bonding modes.



**Figure 1.** Surface morphology of different powder cold-sprayed coatings: (a) macroscopic morphology; (b–d) microscopic morphology; (e–g) cross-section morphology.

Figure 1d shows the SEM surface morphology of the coating prepared with the Al–Al<sub>2</sub>O<sub>3</sub> mixed powder (particle diameter of 5–75 µm). As can be seen, the Al<sub>2</sub>O<sub>3</sub> hard phase has large particle sizes, the coating surface has uneven particle sizes and the majority of particles exhibit varying degrees of fragmentation and plastic deformation. Some particles



become flat, the particles have a stronger compaction effect on the coating, and the particle bonding is more compact as a result of the wide particle size distribution. Large-sized particles also carry more kinetic energy, which is turned into heat energy and causes partial melting and the formation of metallurgical bonds between the particles. However, oxidation ablation took place on the surfaces of some sections (the black portion in the picture), which raised the coating's oxide content. The bonding mode of the coating is mainly mechanical, and metallurgical bonding provides a reference for the metallurgical bonding of the ceramic powders.

According to the above study,  $\text{Al}_2\text{O}_3$  was added to the Al powder-spraying particles during the cold-spraying process, and the hard particles smashed with the substrate, producing strong plastic deformation and becoming well-joined with the substrate (or deposited coating). The sprayed particles continued to have an impact on the coating as it was being deposited. The particles in this procedure compacted the coating that was applied, increasing its density. The loosely bonded particles were knocked off of the coating's surface, and most broke into smaller particles upon impact. These smaller particles joined with the coating to form a dense coating.

The SEM cross-sectional morphology of the coating made from pure Al powder is shown in Figure 1e. It can be seen that the bonding interface between the coating and the substrate has nearly no flaws, the bonding interface curve fluctuates significantly and the coating and substrate mechanically interlock well. The coating has a generally homogeneous microstructure. There are a few isolated microscopic pores and microcracks that are dispersed throughout the coating as a result of the lack of compaction between the particles. The coating contains white oxides. Al- $\text{Al}_2\text{O}_3$  mixed powder was used to produce the substrate-coating interface, which is nearly defect-free (Figure 1f). High-speed  $\text{Al}_2\text{O}_3$  was implanted into the matrix as hard-phase blasting it, causing the interface curve to vary significantly and creating a strong mechanical interlock with the matrix. The pure Al powder is less oxidized, the coating structure is comparatively consistent and the hard-phase  $\text{Al}_2\text{O}_3$  is spread evenly throughout the coating. Most of the particles broke up to varied degrees as a result of the particles' compression. There are hardly any pores or microcracks inside the covering due to the intense particle-particle bonding. Almost no defects are found at the bonding interface between the coating and the substrate prepared from Al- $\text{Al}_2\text{O}_3$  hybrid powder (Figure 1g). As the hard phase bombarded the substrate at high speed, the high-speed  $\text{Al}_2\text{O}_3$  was lodged there, creating a strong mechanical bond. The coating has a thick microstructure. Due to the high  $\text{Al}_2\text{O}_3$  concentration, the coating has an even dispersion of  $\text{Al}_2\text{O}_3$  particles with a wide size distribution, various degrees of fragmentation and plastic deformation. The covering contains very few pores and microcracks.

### 3.2. Surface Composition

The energy spectra of the cold-sprayed coatings comprising various powder materials were examined using an X-ray energy dispersive spectrometer (EDS). The Al pure powder coating is shown in Figure 2 as having only a weak oxygen diffraction signal. In general, the pure Al particles are not oxidized, and the coating has little oxygen. The primary reason for this is that the spraying particles travel at a speed that is much faster than the speed of sound, which reduces the temperature of the particles and speeds up heat conduction. Additionally, the amount of oxidation of the particles is reduced, as is the amount of time the particles spend in contact with the air. The Al- $\text{Al}_2\text{O}_3$  mixed powder was used to create a coating that has a weak oxygen diffraction peak and particles that are essentially unoxidized. The test results show the diffraction peaks of Si, Ti and other elements. The powder material's inclusion of  $\text{SiO}_2$  and  $\text{TiO}_2$ , which can also improve the coating's wear resistance, is the cause.

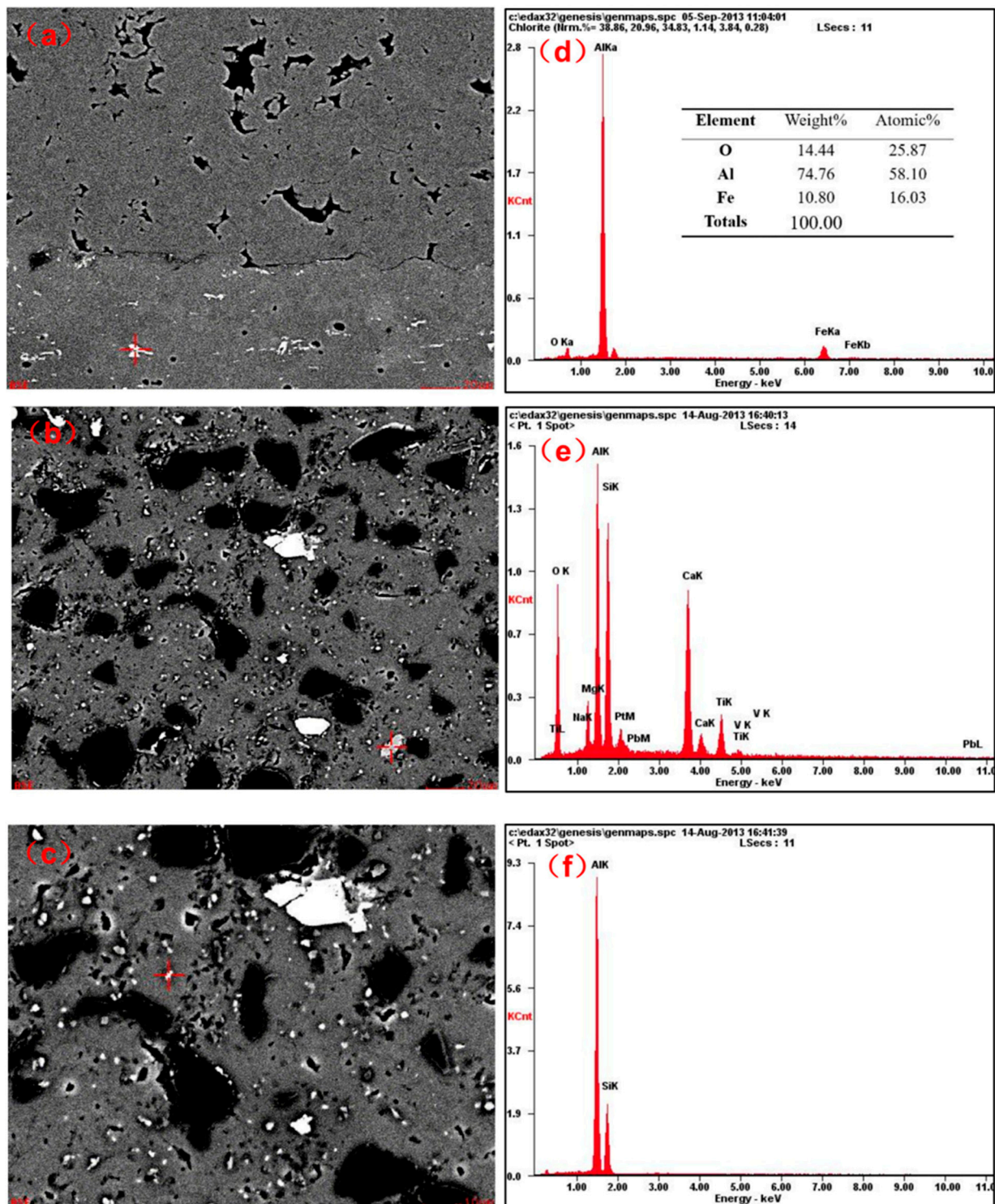
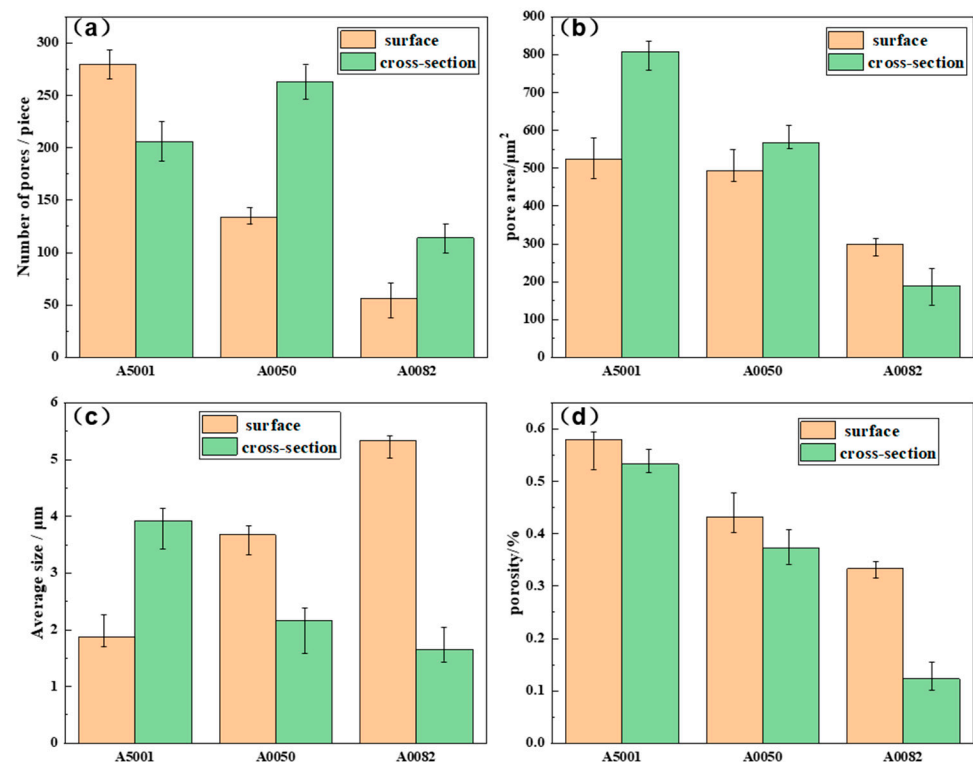


Figure 2. EDS spectra of different cold-sprayed powder material coatings' cross-sections: (a,d) A5001; (b,e) A0050; (c,f) A0082.

### 3.3. Coating Porosity

Figure 3 shows that when the A5001 pure Al powder material is used to make the coating, the porosity of the coating is 0.5792%, but the average size of the pores is small, 1.87  $\mu\text{m}$ . There are 280 pores in the coating. The porosity of the coating is 0.4315%, which is lower than that of the pure Al coating; however, the average size of the pores increases to 3.67  $\mu\text{m}$  when the powder material used is A0050. When the powder material is Al-Al<sub>2</sub>O<sub>3</sub>

of A0082, the  $\text{Al}_2\text{O}_3$  content, size increase, number of pores and porosity of the coating decrease while the average size of the pores remains the same.



**Figure 3.** Surface porosity of coatings prepared by different powders: (a) number of pores; (b) pore area; (c) average pore size; (d) porosity.

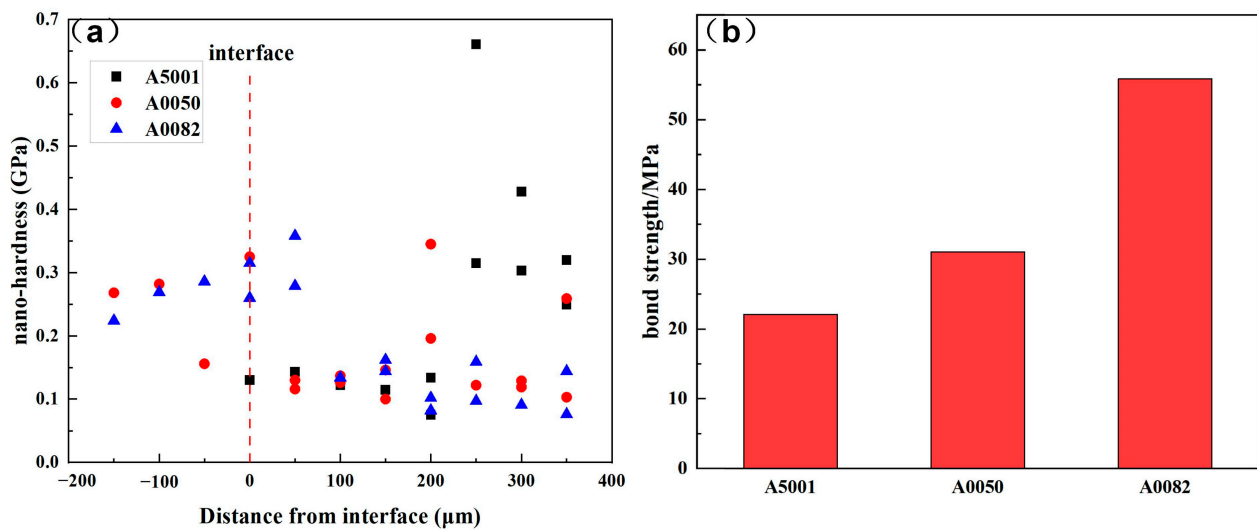
As can be seen, the porosity of the powder material drops following the addition of  $\text{Al}_2\text{O}_3$ , while the pore size rises. The primary explanation for this is that after adding  $\text{Al}_2\text{O}_3$  to the powder material, the coating's porosity decreased and the hard phase's compaction impact increased. However, the sizes and shapes of the varied sizes led to an increase in pore size because  $\text{Al}_2\text{O}_3$  particles have an irregular form and are larger than pure Al particles.

According to Figure 3, the surface pores have the same number of pores, total area, average size and porosity as the cross-sections of the three coatings, but the three coatings have fewer pores overall, a smaller average size and a lower porosity than the surface. The average pore sizes are 3.93  $\mu\text{m}$ , 2.16  $\mu\text{m}$  and 1.66  $\mu\text{m}$ , while the porosities are 0.533%, 0.3727% and 0.1233%, respectively. The primary explanation for this is that the coating is more compact in the vertical plane, which is also the direction in which particles were compacted.

### 3.4. Hardness and Bonding Strength of the Coating

The distribution of the coating's nano-hardness, as measured from the interface distance, is shown in Figure 4a. Near the interface of about 100 m, the coating made from pure Al powder is approximately 0.12 GPa. However, when the distance from the contact increases inside the coating, the nano-hardness gradually rises and can reach 0.5 GPa at a distance of approximately 250–350 m from the interface. The primary reason for this is that as the coating thickness increases, the coating created by particle deposition becomes progressively denser. The Al- $\text{Al}_2\text{O}_3$  mixed powder coating has a nano-hardness of roughly 0.25 GPa at the substrate. The nano-hardness of the coating is about 0.1–0.15 GPa, which is less than the nano-hardness of the pure Al powder coating in the range of 50–350 microns from the interface. The primary cause is a decrease in the coating density that was brought on by the addition of  $\text{Al}_2\text{O}_3$  powder particles.





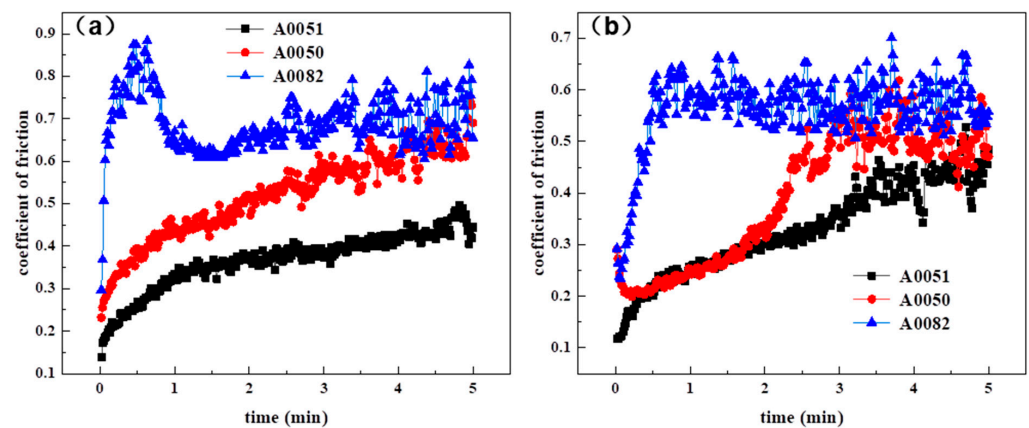
**Figure 4.** Coatings prepared from each of the three powder materials (a) nano-hardness distribution at the interface; (b) bonding strength.

Figure 4b shows that the average bonding strength of the coating made from pure Al powder A5001 is 22.07 MPa, followed by that of the coating made from A0050 powder at 31.05 MPa and the coating made from A0082 powder at 55.82 MPa. As observed, adding  $\text{Al}_2\text{O}_3$  to the powder material strengthens the bond between the substrate and the coating. The bonding strength of the coating dramatically improves as the diameter and quantity of  $\text{Al}_2\text{O}_3$  particles increase. The primary reason for this is that as the amount of  $\text{Al}_2\text{O}_3$  in the coating increases, so do its mass and kinetic energy during deposition. This lowers the porosity by tamping down the layer that was previously placed. The tamping action is improved, and the bonding strength is also significantly increased with an increase in the diameter and composition of  $\text{Al}_2\text{O}_3$  particles.

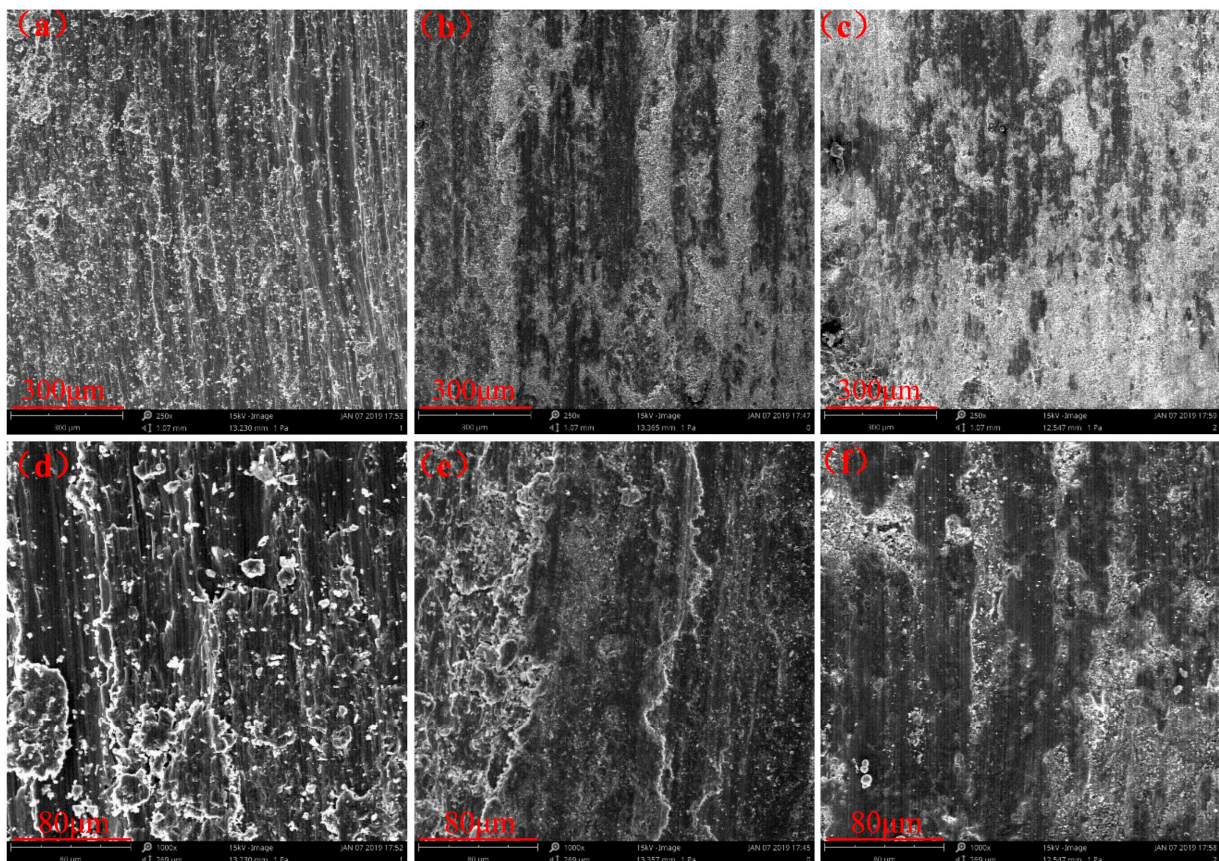
### 3.5. Friction and Wear Properties of the Coating

Figure 5 shows the change in the friction coefficient over time and at various friction frequencies for the three cold-sprayed coatings. The figure shows that the friction coefficient of the coating reduces with an increasing friction frequency, and the law of friction coefficient changing with time is essentially the same for friction frequencies of 2 Hz and 3 Hz. The coefficient of friction of the pure Al coatings is relatively low; however, coatings made with A0050 powder have a higher coefficient of friction than pure Al coatings, and the A0082 powder has the highest coefficient of friction. At the beginning of friction, the coating material's friction coefficient is comparatively low. The pure Al coating's friction coefficient gradually rises with increased friction time. The rising rate is faster in the first period and slower in the second period. The friction coefficient of the coating made from powdered Al- $\text{Al}_2\text{O}_3$  grows quickly before entering a period of relative stability. Additionally, the friction coefficient of a coating made of pure Al varies only slightly during friction, whereas the friction coefficient of a coating made of an Al- $\text{Al}_2\text{O}_3$  mixture undergoes significant variation during friction as a result of the constant peeling of  $\text{Al}_2\text{O}_3$  particles.

The wear morphology of the coating created by various materials is shown in Figure 6. Furrows created by friction can be seen on the wear surface of the coating that was made from pure Al (Figure 6a,d). Uneven furrow distribution, deeper individual furrows and a more significant loss of the coated surface material are all present. Pits for spalling are numerous. Adhesive wear and a small amount of abrasive wear brought on by sliding friction are the two types of wear failure for the coating.



**Figure 5.** Variation of friction coefficient with time under different friction frequencies: (a) 2 Hz; (b) 3 Hz.



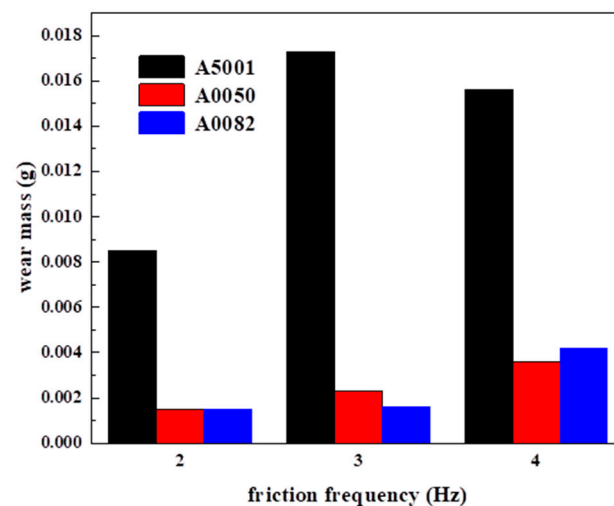
**Figure 6.** The wear scar morphology of cold-sprayed coatings of different powders: (a,d) A5001; (b,e) A0050; (c,f) 0082.

The A0050 powder substance forms black and white furrows on the coating's surface (Figure 6b,e). The white portion is an indication of wear from hard  $\text{Al}_2\text{O}_3$  particles. The depth of the wear marks is less than that of the coating made of pure Al, and its surface is uneven. Abrasive wear is the major type of wear failure for the coating.

The area of white wear markings on the wear surface of the coating that was created using powder A0082 material is larger than the area of white wear markings on the coating created using powder A0050 material (Figure 6c,f). The primary cause for this is that the A0082 powder material has more and larger  $\text{Al}_2\text{O}_3$  particles than the A0050 powder material. Hard  $\text{Al}_2\text{O}_3$  particles act as wear-resistant reinforcing phases during friction,

which can successfully stop wear marks from spreading and increase wear resistance. In addition, the friction causes a dense work-hardening layer to grow on the wear surface, increasing the material's wear resistance.

Figure 7 shows that when the frequency of friction increases, so does the wear mass of the coatings made from the three distinct powder materials. Pure Al coating has the highest wear amount at the same friction frequency. The quantity of wear significantly decreases once the coating is combined with  $\text{Al}_2\text{O}_3$  particles. The experiment shows that adding  $\text{Al}_2\text{O}_3$  particles to the powder mixture boosts the coating's wear resistance. Compared with the previous paper [26], the wear mass in this work is less than the 316L-SiC Composite Coating, indicating a better anti-wear property.



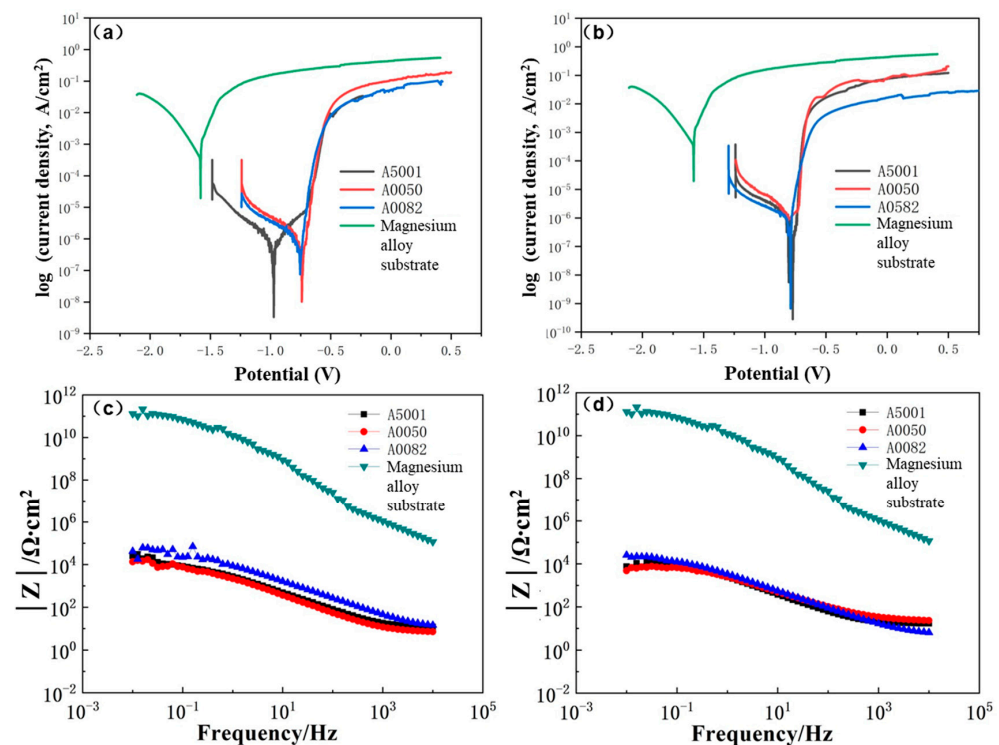
**Figure 7.** Comparison of wear loss of coatings prepared by different materials at different friction frequencies.

### 3.6. Corrosion Property

The polarization curves (Figure 8a,b) show that the corrosion potential of the coating is significantly positively shifted compared to the substrate, and the corrosion current of the coating is reduced by several orders of magnitude after the preparation of 0.5 mm and 1.0 mm thick aluminum-based coatings on the surface of the ZM5 magnesium alloy. This is due to the passivation effect of the aluminum-based coating during the corrosion process. The self-corrosion potential is significantly higher than that of the magnesium alloy substrate, which lowers the rate of metal-on-metal corrosion. The coating helps to protect against the corrosive medium, and the difficulty of the corrosion reaction indicates that it has strong corrosion resistance.

The corrosion potential of the coating made with pure Al powder A5001 is  $-1.0$  V when the coating thickness is 0.5 mm, while the corrosion potential of the coating prepared with the A0050 and A0082 powders is  $-0.75$  V. Its corrosion protection effect is greater than that of a coating made from pure Al powder A5001, and its positive shift value is higher than that of the pure Al powder A5001 coating. The coating created using A0082 powder had the lowest corrosion current and the greatest corrosion resistance of the three coatings. The positive shift of the corrosion potential of the coatings created by the three materials is roughly the same at 1.0 mm in thickness, or  $-0.75$ . The coating made with A0082 powder has the thinnest thickness.












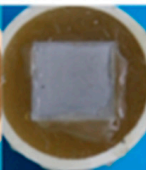

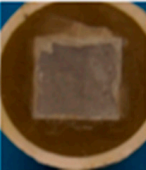


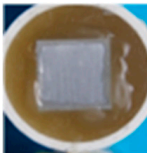
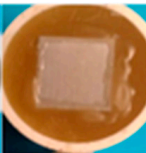
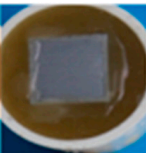
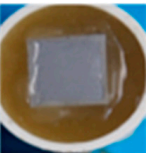
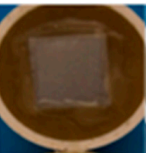

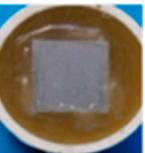
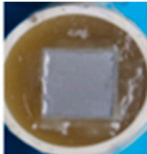

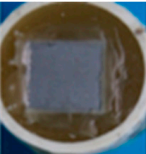
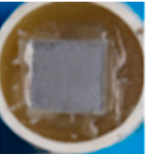

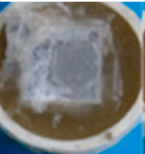


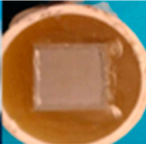
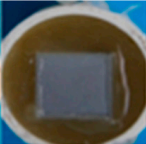
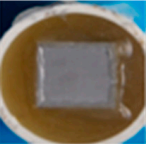
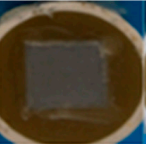
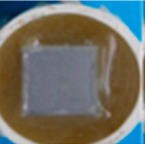
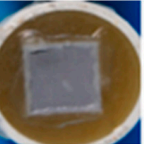

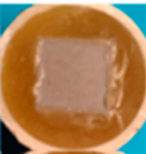
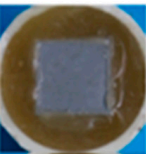
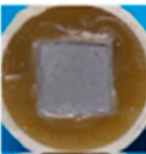
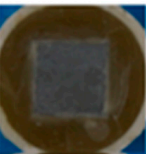
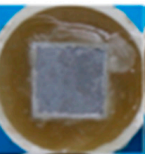
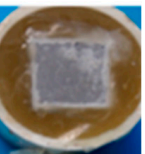



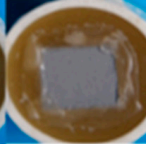
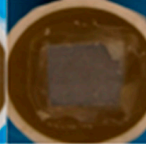
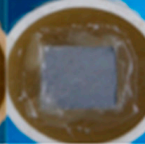
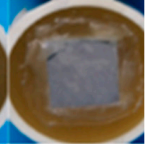


**Figure 8.** Polarization curves and impedance curves of magnesium alloy substrate and coatings with different thicknesses of three powders: (a,c) 0.5 mm; (b,d) 1 mm.

The electrochemical impedance modulus of the coating sample is larger than that of the magnesium alloy substrate sample, as can be seen from the impedance curve (Figure 8c,d). The impedance modulus in the Bode diagram overlaps in the high-frequency region and gradually decreases in the middle- and low-frequency region, indicating a continuous decline in the corrosion resistance of the magnesium alloy substrate and coating during the immersion process, which is an accelerated corrosion process. The coating exhibits greater stability and corrosion resistance, which may effectively protect the substrate material. The corrosion rate of the coating during the corrosion process is lower than that of the magnesium alloy substrate. The coating made from A0082 powder has a greater impedance modulus and provides the optimum corrosion protection effect when the coating thickness is 0.5 mm. The impedance modulus of the coating created by the three powders is comparable when the coating thickness is 1.0 mm. It can be seen that when the coating thickness is thick enough, the corrosion protection effect of the coatings prepared by the three coating materials is equivalent.

Table 3 displays the macroscopic morphology of salt-spray corrosion on the coating produced by the substrate and three different materials. The results show that after 24 h of salt-spray corrosion, the magnesium alloy samples started to show apparent corrosion. There were corrosion products on the surface, and the corrosion effect grew worse as the salt spray time increased. Under identical salt spray conditions, the pure Al coating sample's surface deteriorated less quickly. At 192 h of salt-spray corrosion, the coating's surface, with a thickness of 0.5 mm, started to bulge as the time increased. The corrosion was severe at 288 h and 500 h.

**Table 3.** Macroscopic corrosion morphology of the substrate and the three coatings after salt-spray corrosion.

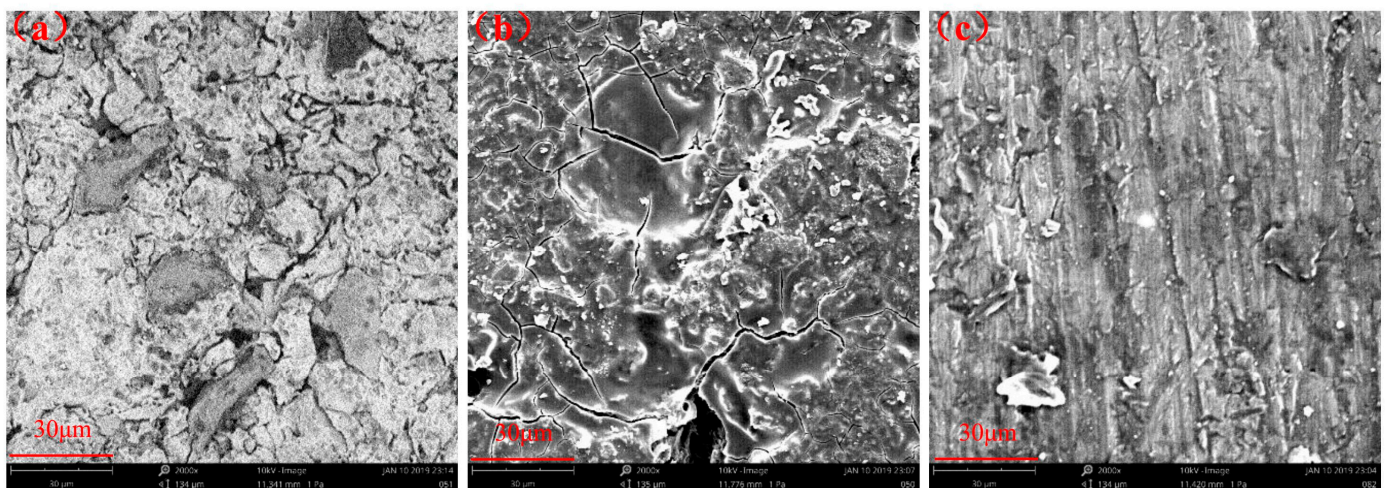
|       |           | Time/h  |   |   |  |   |   |   |
|-------|-----------|---|---|---|--|---|---|---|
|       |           | 0   | 24  | 48  | 96   | 192   | 288   | 500   |
|       | Substrate |    |    |    |    |    |    |    |
|       |           |   |   |   |  |   |   |   |
| A5001 | 0.5 mm    |    |    |    |    |    |    |    |
|       | 1.0 mm    |    |    |    |    |    |    |    |
| A0500 | 0.5 mm    |  |  |  |  |  |  |  |
|       | 1.0 mm    |  |  |  |  |  |  |  |
| A0082 | 0.5 mm    |  |  |  |  |  |  |  |
|       | 1.0 mm    |  |  |  |  |  |  |  |

White corrosion products with a thickness of 0.5 mm, which were created by the A0050 powder, started to emerge all around the coating after 192 h of salt-spray corrosion. After 500 h of corrosion, a significant amount of white oxides were generated on the surface, badly harming the coating. The surface protection layer of the coating with a thickness of 1 mm showed pitting corrosion products after 500 h of corrosion. After 288 h of salt-spray corrosion, the coating with a thickness of 0.5 mm that was created by the A0082 powder started to show visible white corrosion products around the sample. More white oxidation corrosion products were formed on the surface after 500 h of corrosion. After

500 h of corrosion, the surface of the 1 mm thick coating started to show punctate corrosion products, but the coating held up well and continued to function as a protective layer.

From a comparison of the corrosion resistance of the coatings made from three different materials, it can be seen that the pure Al coating exhibits more severe corrosion when the coating thickness is 0.5 mm and the corrosion time is 288 h, while the coatings made from the A0050 powder and the A0082 powder exhibit only minor corrosion. This demonstrates how increasing the amount of  $\text{Al}_2\text{O}_3$  particles in the powder composition improves the coating's corrosion resistance. The coating made from the A0082 powder material, which has larger particles and more  $\text{Al}_2\text{O}_3$  in it, has a stronger corrosion resistance than the coating made from the A0050 powder material. The key factor is that the coating is denser and has a higher compaction effect with the addition of the  $\text{Al}_2\text{O}_3$  particles. The corrosion resistance of the coating is improved by the  $\text{Al}_2\text{O}_3$  particles' greater corrosion resistance. The aforementioned experimental findings demonstrate that the application of an Al-based coating to the surface of a magnesium alloy can have a very positive protective effect on the matrix and can significantly increase its ability to resist corrosion. The thickness of the coating affects how resistant it is to corrosion. The thick coating has a better protective impact on the substrate and has a significantly higher corrosion resistance than the thin coating.

After 48 h of salt-spray corrosion, the SEM morphology of the coatings created by three different powder materials is shown in Figure 9. The figure shows that the pure Al coating made from the A5001 powder material has a minimal pitting density and little pitting depth on the coating surface at the initial stage of corrosion, and the coating performs well as a protective layer. After 48 h of salt-spray corrosion, corrosion microcracks and a tiny quantity of corrosion products emerged at the interface of the particles, and under the influence of internal tension, the coating made from A0050 powder material split into blocks. The coating made from A0082 powder material was corroded after 48 h of exposure to salt spray, but there were no corrosion microcracks or byproducts, and its protective function was better.



**Figure 9.** SEM morphology of the coatings after 48 h of salt-spray corrosion: (a) A5001; (b) A0050; (c) A0082.

#### 4. Conclusions

In this study, ZM5 magnesium alloy was cold-sprayed with pure aluminum and aluminum- $\text{Al}_2\text{O}_3$  coatings. Studies were conducted on the coatings' internal structure, phase structure, surface morphology, bonding strength, tribological capabilities and corrosion resistance. The main conclusions are as follows:

- (1) A coating with a typically homogenous microstructure, a low oxygen content, almost no oxidation of the Al powder, 0.92% porosity and a dense structure is made using



pure aluminum powder. Once the powder material and  $\text{Al}_2\text{O}_3$  are mixed, the porosity of the coating can be further reduced. The hard phase significantly increases the coating's hardness. The particles are linked together metallurgically. By combining metallurgical bonding and mechanical interlocking, the coating bonds.

- (2) The nano-hardness of pure aluminum coating is approximately 0.5 GPa. The nano-hardness and bonding strength of the coating are improved after  $\text{Al}_2\text{O}_3$  is added to the powder material. The wear-resistant reinforcement phase, which consists of tough  $\text{Al}_2\text{O}_3$  particles, can effectively slow the development of wear marks and provide a layer of work hardening on the wear surface to strengthen the material's wear resistance. The wear mass grows in tandem with an increase in the friction frequency, and the friction coefficient of the three coatings decreases. With the same friction frequency, pure aluminum coverings experience the most wear loss.
- (3) The three Al-based coatings have a significantly lower electrochemical impedance modulus and corrosion current than the substrate. The coating made with A0082 powder has the least amount of corrosion current. To improve corrosion resistance, a specific percentage of  $\text{Al}_2\text{O}_3$  particles is added to the coating. The ability of a coating to resist corrosion is proportional to its thickness. When the coating thickness is 0.5 mm, the coating made from A0082 powder provides the best corrosion protection. The thick coating protects the substrate more effectively and has significantly higher corrosion resistance than the thin coating.

**Author Contributions:** Conceptualization, G.H.; Methodology, S.C., T.W., J.H., X.C., C.Y. and S.Z.; Formal analysis, S.C., T.W., S.X., C.F., W.D. and Q.W.; Investigation, S.C. and Q.W.; Resources, J.H., Z.C. and D.D.; Data curation, D.C.; Writing—original draft, D.C.; Visualization, Q.L.; Supervision, G.H.; Funding acquisition, Q.W. All authors have read and agreed to the published version of the manuscript.

**Funding:** The authors gratefully acknowledge financial support from the Guang Dong Basic and Applied Basic Research Foundation (2020B1515120027), the National Defense Science and Technology Key Laboratory Fund (6142005180203), Fangchenggang Scientific Research and Technology Development Project (AB21014008), Wuhu Science and Technology Major Project (Grant No. 2021zd08), and Anhui Unveiled Project (Grant No: JB21049).

**Institutional Review Board Statement:** Not applicable.

**Informed Consent Statement:** Not applicable.

**Data Availability Statement:** Data sharing is not applicable to this article.

**Conflicts of Interest:** The authors declare no conflict of interest.

## References

1. Song, J.; Chen, J.; Xiong, X.; Peng, X.; Chen, D.; Pan, F. Research advances of magnesium and magnesium alloys worldwide in 2021. *J. Magnes. Alloy.* **2022**, *10*, 863–898. [\[CrossRef\]](#)
2. Song, J.; She, J.; Chen, D.; Pan, F. Latest research advances on magnesium and magnesium alloys worldwide. *J. Magnes. Alloy.* **2020**, *8*, 1–41. [\[CrossRef\]](#)
3. Gonzaga, S.; Molina, A.; Guardiola, R.; Martínez, H.; Vélez, E.V.; Tapia, J.S. Synthesis of Magnesium-Based Alloys by Mechanical Alloying for Implant Applications. *Coatings* **2023**, *13*, 260. [\[CrossRef\]](#)
4. Yan, C.; Xin, Y.; Chen, X.-B.; Xu, D.; Chu, P.K.; Liu, C.; Guan, B.; Huang, X.; Liu, Q. Evading strength-corrosion tradeoff in Mg alloys via dense ultrafine twins. *Nat. Commun.* **2021**, *12*, 4616. [\[CrossRef\]](#) [\[PubMed\]](#)
5. Lu, X.; Li, Y.; Ju, P.; Chen, Y.; Yang, J.; Qian, K.; Zhang, T.; Wang, F. Unveiling the inhibition mechanism of an effective inhibitor for AZ91 Mg alloy. *Corros. Sci.* **2019**, *148*, 264–271. [\[CrossRef\]](#)
6. Mégret, A.; Prince, L.; Olivier, M.-G.; Vitry, V. Tribo- and Tribocorrosion Properties of Magnesium AZ31 Alloy. *Coatings* **2023**, *13*, 448. [\[CrossRef\]](#)
7. Magdum, R.; Chinnaiyan, P. Experimental Investigation and Optimization of AZ31 Mg alloy during Warm Incremental Sheet Forming to Study Fracture and Forming Behaviour. *Coatings* **2023**, *13*, 68. [\[CrossRef\]](#)
8. Zhang, D.; Peng, F.; Liu, X. Protection of magnesium alloys: From physical barrier coating to smart self-healing coating. *J. Alloys Compd.* **2021**, *853*, 157010. [\[CrossRef\]](#)

9. Liu, Q.; Chen, D.; Kang, Z. One-Step Electrodeposition Process To Fabricate Corrosion-Resistant Superhydrophobic Surface on Magnesium Alloy. *ACS Appl. Mater. Interfaces* **2015**, *7*, 1859–1867. [\[CrossRef\]](#)
10. Fattah-alhosseini, A.; Chaharmahali, R.; Babaei, K. Impressive strides in amelioration of corrosion and wear behaviors of Mg alloys using applied polymer coatings on PEO porous coatings: A review. *J. Magnes. Alloy.* **2022**, *10*, 1171–1190. [\[CrossRef\]](#)
11. Di Egidio, G.; Tonelli, L.; Morri, A.; Boromei, I.; Shashkov, P.; Martini, C. Influence of Anodizing by Electro-Chemical Oxidation on Fatigue and Wear Resistance of the EV31A-T6 Cast Magnesium Alloy. *Coatings* **2023**, *13*, 62. [\[CrossRef\]](#)
12. Singh, N.; Batra, U.; Kumar, K.; Siddiquee, A.N. Evaluating the Electrochemical and In Vitro Degradation of an HA-Titania Nano-Channeled Coating for Effective Corrosion Resistance of Biodegradable Mg Alloy. *Coatings* **2023**, *13*, 30. [\[CrossRef\]](#)
13. Li, B.; Yin, X.; Xue, S.; Mu, P.; Li, J. Facile fabrication of graphene oxide and MOF-based superhydrophobic dual-layer coatings for enhanced corrosion protection on magnesium alloy. *Appl. Surf. Sci.* **2022**, *580*, 152305. [\[CrossRef\]](#)
14. Zhai, H.; Yuan, H.; Li, W.; Zhang, X.; Li, X.; Cai, A. Corrosion resistance mechanisms of detonation sprayed Fe-based amorphous coating on AZ31B magnesium alloy. *J. Non Cryst. Solids* **2022**, *576*, 121276. [\[CrossRef\]](#)
15. Wang, B.; Liu, X.; Wang, Y.; Ding, J.; Wei, S.; Xia, X.; Liu, M.; Xu, B. Microstructure and Anti-Corrosion Properties of Supersonic Plasma Sprayed Al-Coating with Nano-Ti Polymer Sealing on Az91-Magnesium Alloy. *J. Mater. Res. Technol.* **2022**, *21*, 2730–2742. [\[CrossRef\]](#)
16. Daroonparvar, M.; Bakhsheshi-Rad, H.R.; Saberi, A.; Razzaghi, M.; Kasar, A.K.; Ramakrishna, S.; Menezes, P.L.; Misra, M.; Ismail, A.F.; Sharif, S.; et al. Surface modification of magnesium alloys using thermal and solid-state cold spray processes: Challenges and latest progresses. *J. Magnes. Alloy.* **2022**, *10*, 2025–2061. [\[CrossRef\]](#)
17. Wei, Y.-K.; Luo, X.-T.; Ge, Y.; Chu, X.; Huang, G.-S.; Li, C.-J. Deposition of fully dense Al-based coatings via in-situ micro-forging assisted cold spray for excellent corrosion protection of AZ31B magnesium alloy. *J. Alloys Compd.* **2019**, *806*, 1116–1126. [\[CrossRef\]](#)
18. Zhu, J.; Cheng, X.; Zhang, L.; Hui, X.; Wu, Y.; Zheng, H.; Ren, Z.; Zhao, Y.; Wang, W.; Zhu, S.; et al. Microstructures, wear resistance and corrosion resistance of CoCrFeNi high entropy alloys coating on AZ91 Mg alloy prepared by cold spray. *J. Alloys Compd.* **2022**, *925*, 166698. [\[CrossRef\]](#)
19. Luo, X.; Wei, Y.; Shen, J.; Ma, N.; Li, C.-J. Breaking the trade off between corrosion resistance and fatigue lifetime of the coated Mg alloy through cold spraying submicron-grain Al alloy coatings. *J. Magnes. Alloy.* **2023**, *in press*. [\[CrossRef\]](#)
20. Mouli, G.C.; Chakradhar, R.P.S.; Srivastava, M.; Barshilia, H.C. Cold-Sprayed Cu-Zn-Al<sub>2</sub>O<sub>3</sub> Coating on Magnesium Alloy: Enhanced Microhardness and Corrosion Behavior. *J. Mater. Eng. Perform.* **2022**. [\[CrossRef\]](#)
21. Liu, Y.; Tan, G.; Tang, J.; Zhang, L.; Shen, G.z.; Gu, Z.; Jie, X. Enhanced corrosion and wear resistance of Zn-Ni/Cu-Al<sub>2</sub>O<sub>3</sub> composite coating prepared by cold spray. *J. Solid State Electrochem.* **2023**, *27*, 439–453. [\[CrossRef\]](#)
22. Mohankumar, A.; Duraisamy, T.; Chidambaramseshadri, R.; Pattabi, T.; Ranganathan, S.; Kaliyamoorthy, M.; Balachandran, G.; Sampathkumar, D.; Rajendran, P.R. Enhancing the Corrosion Resistance of Low Pressure Cold Sprayed Metal Matrix Composite Coatings on AZ31B Mg Alloy through Friction Stir Processing. *Coatings* **2022**, *12*, 135. [\[CrossRef\]](#)
23. Spencer, K.; Fabijanec, D.M.; Zhang, M.X. The use of Al-Al<sub>2</sub>O<sub>3</sub> cold spray coatings to improve the surface properties of magnesium alloys. *Surf. Coat. Technol.* **2009**, *204*, 336–344. [\[CrossRef\]](#)
24. Wang, Q.; Spencer, K.; Birbilis, N.; Zhang, M.-X. The influence of ceramic particles on bond strength of cold spray composite coatings on AZ91 alloy substrate. *Surf. Coat. Technol.* **2010**, *205*, 50–56. [\[CrossRef\]](#)
25. Chakradhar, R.P.S.; Chandra Mouli, G.; Barshilia, H.; Srivastava, M. Improved Corrosion Protection of Magnesium Alloys AZ31B and AZ91 by Cold-Sprayed Aluminum Coatings. *J. Therm. Spray Technol.* **2021**, *30*, 371–384. [\[CrossRef\]](#)
26. Chen, J.; Ma, B.; Liu, G.; Song, H.; Wu, J.; Cui, L.; Zheng, Z. Wear and Corrosion Properties of 316L-SiC Composite Coating Deposited by Cold Spray on Magnesium Alloy. *J. Therm. Spray Technol.* **2017**, *26*, 1381–1392. [\[CrossRef\]](#)

**Disclaimer/Publisher’s Note:** The statements, opinions and data contained in all publications are solely those of the individual author(s) and contributor(s) and not of MDPI and/or the editor(s). MDPI and/or the editor(s) disclaim responsibility for any injury to people or property resulting from any ideas, methods, instructions or products referred to in the content.